Loughborough
University

This item was submitted to Loughborough's Institutional Repository (https://dspace.lboro.ac.uk/) by the author and is made available under the following Creative Commons Licence conditions.

For the full text of this licence, please go to:
http://creativecommons.org/licenses/by-nc-nd/2.5/

[10] M. Nagao and T. Matsuyama, "Edge preserving smoothing," *Comput. Graph. Image Process.,* vol. 9, pp. 394–407, Apr. 1979.

[11] W. E. Higgins, "A flexible implementation of maximum-homogeneity filtering for 2-D and 3-D images," *IEEE Trans. Signal Processing,* vol. 39, pp. 2325–2331, Oct. 1991.

[12] P. Perona and J. Malik, "Scale-space and edge detection using anisotropic diffusion," *IEEE Trans. Pattern Anal. Machine Intell.,* vol. 12, pp. 629–639, June 1990.

[13] Y. You, W. Xu, A. Tannenbaum, and M. Kaveh, "Behavioral analysis of anisotropic diffusion in image processing," *IEEE Trans. Image Processing,* vol. 5, pp. 1539–1553, Nov. 1996.

[14] J. Serra, *Image Analysis and Mathematical Morphology.*   New York: Academic, 1982, vol. 1.

[15] F. Meyer and S. Beucher, "Morphological segmentation," *J. Vis. Commun. Image Represent.,* vol. 1, pp. 21–46, Sept. 1990.

[16] W. E. Higgins and E. J. Ojard, "Interactive morphological watershed analysis for 3D medical images," *Comput. Med. Imag. Graph.: Special Issue Adv. 3D Image Process. Medicine,* vol. 17, pp. 387–395, July–Oct. 1993.

[17] M. W. Hansen and W. E. Higgins, "Relaxation methods for supervised image segmentation," *IEEE Trans. Pattern Anal. Machine Intell.,* vol. 19, pp. 949–962, Sept. 1997.

[18] L. Vincent and P. Soille, "Watersheds in digital spaces: An efficient algorithm based on immersion simulations," *IEEE Trans. Pattern Anal. Machine Intell.,* vol. 13, pp. 583–598, June 1991.

[19] J. Canny, "A computational approach to edge detection," *IEEE Trans. Pattern Anal. Machine Intell.,* vol. PAMI-8, pp. 679–698, Nov. 1986.

An Enhanced NAS-RIF Algorithm for Blind Image Deconvolution

Chin Ann Ong and Jonathon A. Chambers

Abstract— We enhance the performance of the nonnegativity and support constraints recursive inverse filtering (NAS-RIF) algorithm for blind image deconvolution. The original cost function is modified to overcome the problem of operation on images with different scales for the representation of pixel intensity levels. Algorithm resetting is used to enhance the convergence of the conjugate gradient algorithm. A simple pixel classification approach is used to automate the selection of the support constraint. The performance of the resulting enhanced NAS-RIF algorithm is demonstrated on various images.

Index Terms—Blind image deconvolution, classification, conjugate gradient, deblurring.

I. Introduction

In many applications images are degraded by blur and additive noise, for example in astronomy, medical imaging, and remote sensing [1]–[3]. Such degradation is commonly represented by a

linear model of the form

$$g(x,y) = f(x,y) * h(x,y)$$
$$= \sum_{(n,m)} f(n,m)h(x-n,y-m) + n(x,y) \qquad (1)$$

where $g(x,y)$, $f(x,y)$, and $h(x,y)$, denote respectively the degraded two-dimensional (2-D) image, the true image and the linear shift-invariant blur, morecommonly referred to as the point-spread function (PSF); $*$ denotes the 2-D convolution operation, $n(x,y)$ is the additive noise and x, y, n, $m \in Z$, the set of integers.

The problem of blind image deconvolution corresponds to estimating the true image, $f(x,y)$, from the observed image $g(x,y)$, when both $f(x,y)$ and the PSF, $h(x,y)$, are either unknown or partially known. This is a difficult ill-conditioned and ill-posed problem due to the existence of the additive noise. Direct inversion of the PSF will generally yield high frequency amplification of the additive noise, thereby corrupting the estimate of the true image.

There are two main classes of methods for blind deconvolution. The first class estimates the PSF before estimating the true image. Methods which belong to this class have the advantage of being low complexity approaches, but are limited to situations where the true image, and/or the PSF, are known to have special characteristics [1]. The second class, which is more generally applicable, estimates simultaneously the PSF and true image. Techniques from this second class can be further divided into parametric and nonparametric methods. The parameteric methods assume some model for the PSF or true image, for example an autoregressive (AR) model for the true image and a moving average (MA) model for the PSF, but have practical restrictions and convergence problems [1]. In this work, we therefore concentrate upon a nonparametric method which utilizes only deterministic constraints on the true image such as nonnegativity and known finite support. The iterative blind deconvolution (IBD) algorithm proposed by Ayers and Dainty [4] is an early example of this approach, but this method is known to be unreliable, with problems in uniqueness of solution and convergence, despite noise robustness due to its analogy with Wiener-filtering. Another approach proposed by McCallum [5] is based upon a multimodal cost function, minimized with a simulated annealing algorithm. This algorithm is however too computationally complex for real-time applications, the complexity for each iteration of the algorithm is $O(N_f^4)$ where N_f is the number of pixels within the image estimate.

A new technique belonging to this nonparametric class of blind deconvolution algorithms is the nonnegativity and support constraints recursive inverse filtering (NAS-RIF) algorithm proposed by Kundur and Hatzinakos [1], which was designed to have good convergence properties and relatively low computational complexity, $O(N_f N_u N_{ls,k})$ where N_u is the number of parameters of a 2-D finite impulse response (FIR) filter used to model the inverse of the PSF and $N_{ls,k}$ is the number of line searches used within the conjugate gradient algorithm at the kth iteration of the minimization of an associated cost function. This algorithm also assumes that both the PSF and its inverse are absolutely summable [1]; but, advantageously, is not limited to finite extent PSF's.

In this correspondence we propose modifications to the original NAS-RIF algorithm to overcome some of the limitations found in its operation, namely it is unable to deal robustly with variations in gray-scale ranges, compromises accuracy of restoration with speed of convergence, and requires an accurate estimate of the support of the object of interest.
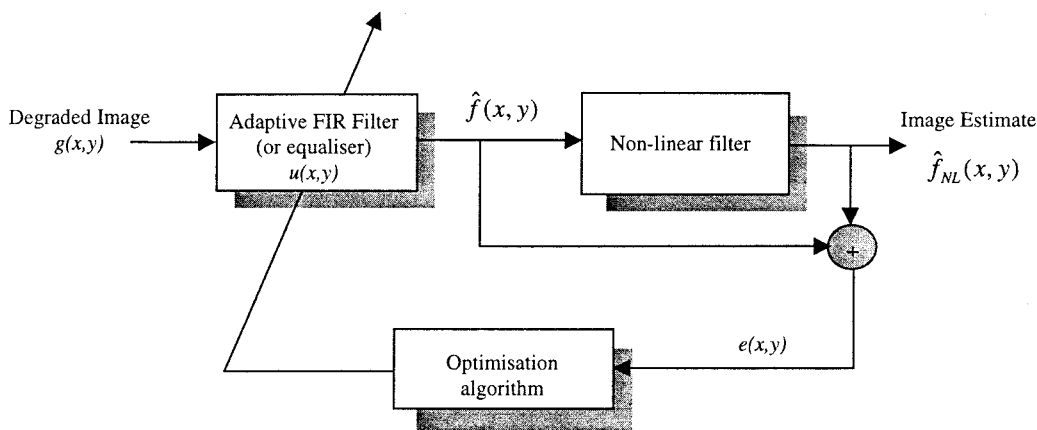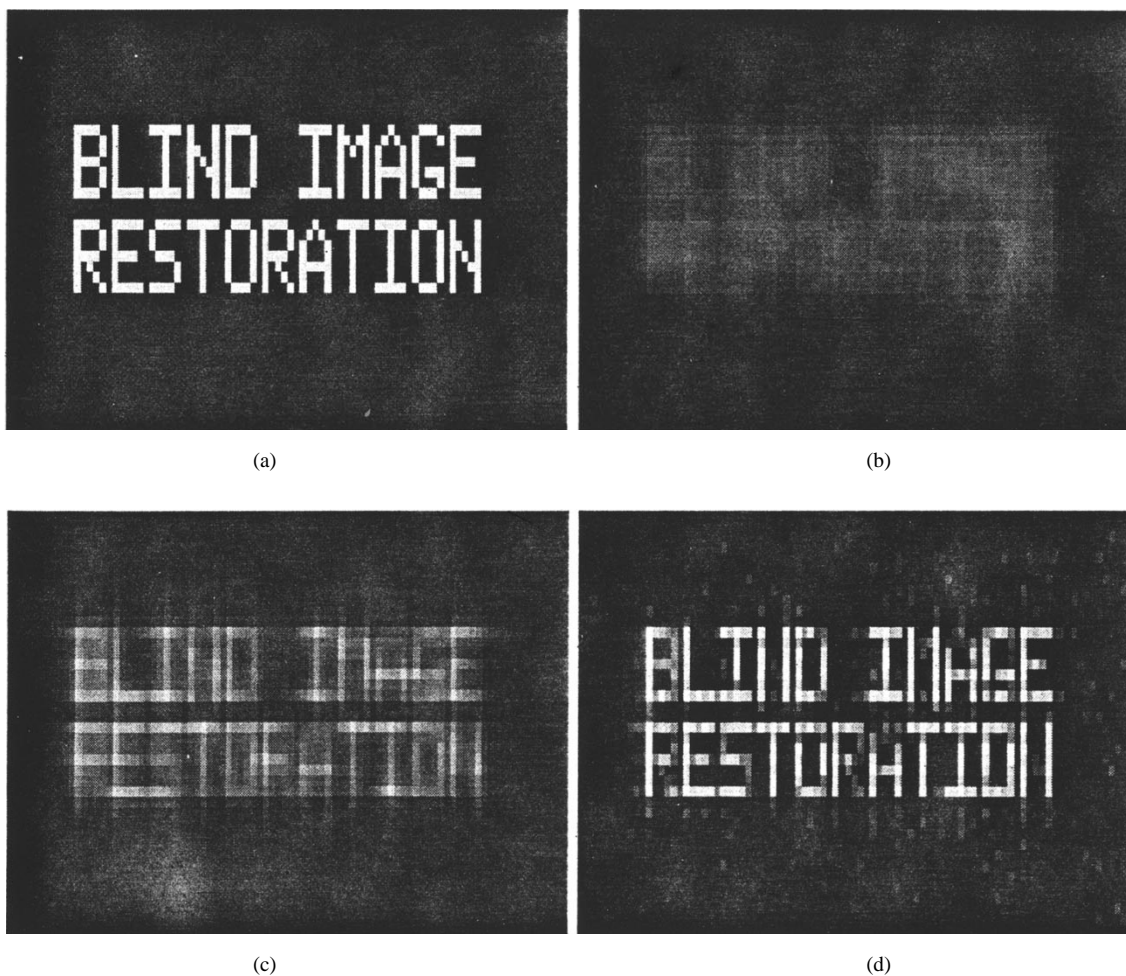
Fig. 1. Structure of the NAS-RIF algorithm.

(a)

(b)

(c)

(d)

Fig. 2. (a) Original image, (b) degraded image, and the image estimates using (c) the original and (d) the enhanced NAS-RIF algorithm.

II. NAS-RIF Algorithm

The structure of the NAS-RIF algorithm is shown in Fig. 1. The true image, $f(x, y)$ in (1), is assumed to contain an object with known finite support against an uniformly black, grey or white background; the object being entirely encompassed within the image. The degraded image, $g(x, y)$, forms the input to an adaptive FIR filter, the output of which, $\hat{f}(x, y)$, is an unconstrained estimate of the true image. The nonlinear filter projects the estimate of the true image onto the space of images which satisfy the nonnegativity and support constraints to form the refined image estimate $\hat{f}_{NL}(x, y)$. That is, pixels in $\hat{f}(x, y)$ which are outside of the region of support of the object are set to the

Fig. 3.   (a) Original image, (b) degraded image, and the image estimates using (c) the original and (d) the enhanced NAS-RIF algorithm.

known background level of the true image, and negative pixels within the region of support of the object are set to zero. The difference between these two images, $e(x, y)$, is the input to the optimization algorithm which minimizes the following cost function

$$J\{u(x,y)\} = \sum_{\forall(x,y)} e^2(x,y)$$
$$= \sum_{\forall(x,y)\in D_{\text{sup}}} \hat{f}^2(x,y)\left[\frac{1 - \text{sgn}(\hat{f}(x,y))}{2}\right]$$
$$+ \sum_{\forall(x,y)\in \bar{D}_{\text{sup}}} [\hat{f}(x,y) - L_B]^2 \qquad (2)$$

where $u(x,y)$ denotes the parameters of the adaptive FIR filter, $\hat{f}(x,y) = g(x,y)*u(x,y)$, D_{sup} is the set of pixels within the known region of support of the object, and $\bar{D}_{\text{sup}}$ is the set of pixels within the image that are outside of the region of support. The parameter L_B corresponds to the background grey-level of the pixels within $\bar{D}_{\text{sup}}$, and $\text{sgn}(x)$ is the sign function. This cost function has been shown to be convex with respect to $u(x,y)$ [6] and has been minimized with the conjugate gradient algorithm. A complete listing of the NAS-RIF algorithm based upon conjugate gradient algorithm minimization of (2) together with some simulation studies can be found in [1].

When the background of the true image is black, i.e., $L_B = 0$, an additional term is added to the cost function (2), of the form $\gamma[\sum_{\forall(x,y)} u(x,y) - 1]^2$, to avoid a trivial all-zero minimum solution, where γ is a positive constant.

III. Enhancing the NAS-RIF Algorithm

In this section we propose modifications to the original NAS-RIF algorithm to enhance its operation.

A. Scaling

The representation of grey-scale intensity levels is arbitrary, for example the closed set of real numbers $[0, 1]$ or $[0, 1000]$ may be used. The original NAS-RIF algorithm based upon the minimization of (2), $L_B \neq 0$, fails to converge because as the algorithm progresses, the d.c. gain of the adaptive FIR filter is not constrained to unity. A scaling difference between the pixel intensity levels of the input $g(x,y)$ and output $\hat{f}(x,y)$ is therefore introduced. The original cost function (2) does not account for such scaling and hence the convergence of the NAS-RIF algorithm is found to be poor [7].

To overcome this limitation, we introduce a scaling term within the cost function of the enhanced NAS-RIF algorithm to compensate for the nonunity d.c. gain of the adaptive filter

$$J\{u(x,y)\} = \sum_{\forall(x,y)\in D_{\text{sup}}} \hat{f}^2(x,y)\left[\frac{1 - \text{sgn}(\hat{f}(x,y))}{2}\right]$$
$$+ \sum_{\forall(x,y)\in \bar{D}_{\text{sup}}} [\hat{f}(x,y) - \alpha L_B]^2 \qquad (3)$$

where $\alpha = \sum_{(x,y)} u(x,y)$ is the d.c. gain of the adaptive filter which ensures that L_B is appropriately scaled in the calculation of the error term during the optimization procedure. The second term in (3) remains quadratic in the parameters of the adaptive filter and
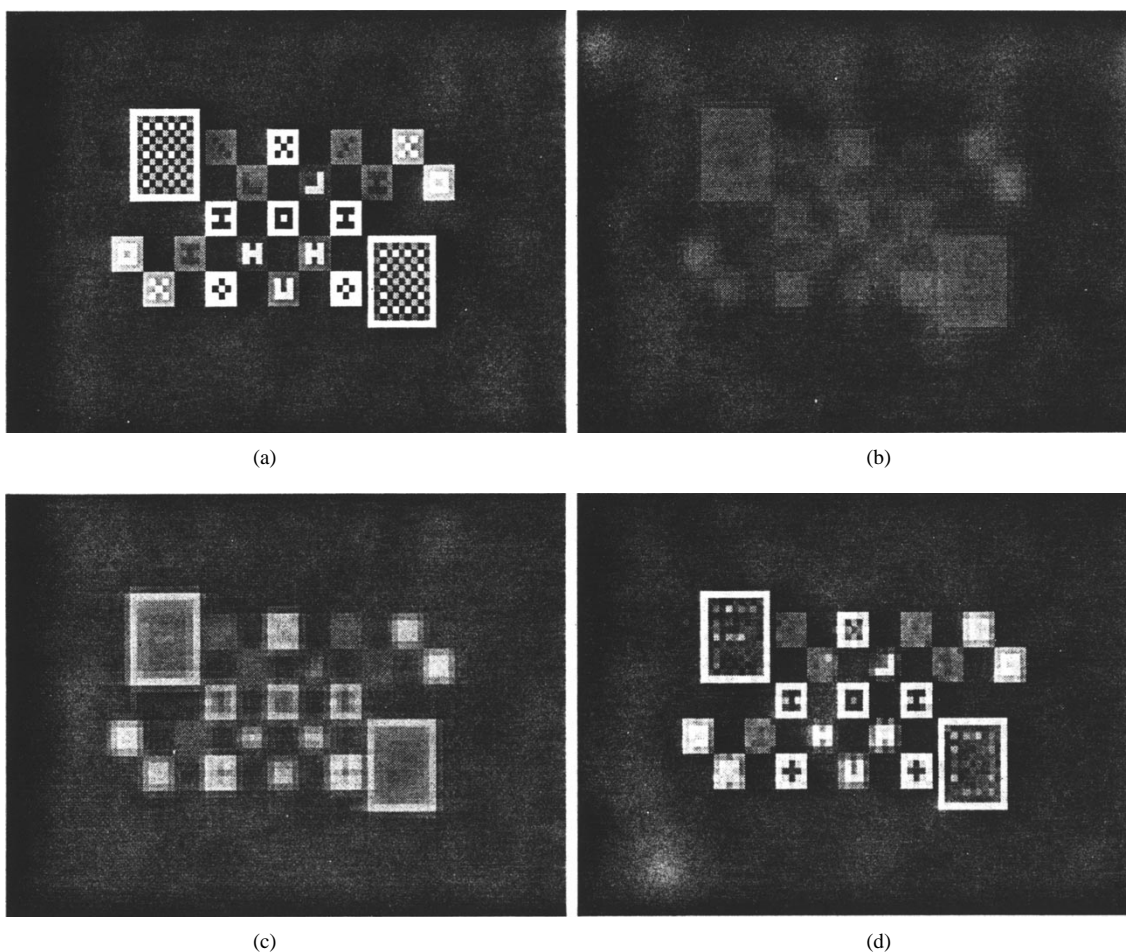
Fig. 4. (a) Original image, (b) degraded image, and the image estimates using (c) original and (d) the enhanced NAS-RIF algorithm.
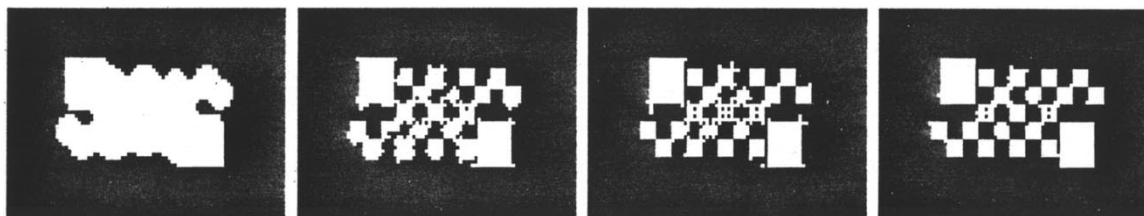

Fig. 5. Evolution of the binary mask $b(x, y)$.

therefore the convex form of the original cost function is maintained. This modification introduces only $O(N_u)$ additional computational complexity to each iteration of the minimization algorithm.

B. Algorithm Resetting

The conjugate gradient algorithm is designed for quadratic cost functions, for more general and nonlinear cost functions, as in (2) and (3), modifications are necessary to aid convergence behavior and encourage convergence to the global minimum [8]. In the enhanced NAS-RIF algorithm we employ algorithm resetting to improve the convergence properties.

For a quadratic cost function of N variables the conjugate gradient algorithm is guaranteed to converge in N iterations. Therefore, in the enhanced NAS-RIF algorithm, due to the nonquadratic nature of (2) and (3), we propose using the partial conjugate gradient algorithm [8], in which the search direction of the conjugate gradient algorithm

is reset to that of the steepest descent algorithm at every N iterations, where N is the number of parameters being estimated. We have also found advantage in increasing progressively the size of the support of adaptive FIR filter during the minimization procedure, beginning with a small support, say 3×3, and adding pixels to the boundary of the support to build up to the target dimension [7].

C. Classification of the Region of Support

In the conventional NAS-RIF algorithm the object is assumed to be contained within a rectangular region of support. However, for nonrectangular objects the real background pixels within the region of support will be wrongly classified as object pixels. This degrades the quality of restoration [7]. We therefore propose to use a simple approach to classify the pixels of the degraded image, $g(x, y)$, as belonging to D_{sup} or $\bar{D}_{\text{sup}}$, other more sophisticated techniques can be found in [9] and [10].

We form a binary mask of $b(x,y)$ of the degraded image $g(x,y)$ based upon a fixed threshold T, that is

$$b(x,y) = \begin{cases} 1, & \text{if } g(x,y) > T \\ 0, & \text{if } g(x,y) \leq 0 \end{cases}.$$

The threshold can easily be found from the image histogram, as it is assumed that the background intensity of the original image $h(x,y)$ is constant, the first mode of the histogram of $g(x,y)$ is therefore likely to be equal to the background intensity, and as such the threshold T can be chosen just above this level. The enhanced NAS-RIF algorithm is therefore based upon the following cost function

$$J\{u(x,y)\} = \sum_{\{(x,y):b(x,y)=1\}} \hat{f}^2(x,y) \left[\frac{1 - \text{sgn}(\hat{f}(x,y))}{2} \right] + \sum_{\{(x,y):b(x,y)=0\}} [\hat{f}(x,y) - \alpha L_B]^2. \tag{4}$$

The mask $b(x,y)$ can be refined during the minimization process using the estimated image $\hat{f}(x,y)$. In terms of computational complexity this will introduce $O(N_f)$ additional threshold tests, together with the computations necessary to form the histogram. In summary, the enhanced NAS-RIF algorithm is based upon the cost function given in (4) minimized with the conjugate gradient algorithm and reinitialization.

IV. Simulations

Three different images are used to compare the performance of the original and enhanced NAS-RIF algorithms. The first image is shown in Fig. 2(a). The degraded image, Fig. 2(b), is produced by using a separable PSF generated from $\underline{v}\underline{v}^T$ where $\underline{v}$ is a column vector, of dimension 23×1, with elements that geometrically decrease from the centre by a factor of 0.7 [1]. Additive white Gaussian noise is also added such that the signal-to-noise (SNR) ratio is 40 dB. The background grey scale level of the original image is set at $1/255$ over a normalized grey scale range of $[0,1]$. The image estimates, shown in Fig. 2(c) and (d), are obtained after 40 iterations. Additional iterations for the modified algorithm yield severe noise amplification, whereas the original algorithm locks-up at the 20th iteration as a result of the nonzero background grey level of the original image. The adaptive FIR filter, u, has dimension 5×5. It is clear that the modified algorithm has improved convergence properties, but there is some amplification of the noise.

In Fig. 3(a), a segmented version of the Lenna image is shown. The same PSF function is applied to this image to generate Fig. 3(b), together with additive white Gaussian noise of 30 dB SNR. The image estimates in Fig. 3(c) and (d) are again obtained after 20 iterations so as to avoid noise amplification. The adaptive FIR filter has dimension 5×5. Notice that the image estimate with the enhanced algorithm is noticeably more sharp and there is little noise amplification as a result of the smoothness of the Lenna image. The key advantage of the NAS-RIF type algorithms is good performance without having to estimate explicitly the PSF.

To show how the region of support is classified automatically, a third image is introduced in Fig. 4(a). Similar degradation is employed to generate the degraded image in Fig. 4(b). The estimated images are shown in Fig. 4(c)–(d), which clearly demonstrates the advantage of the enhanced NAS-RIF algorithm. Finally, the evolution of the binary mask, $b(x,y)$, is shown in Fig. 5.

V. Conclusion

In this work, we have presented three enhancements to overcome drawbacks of the original NAS-RIF algorithm. The problem of robustness to the range of pixel values is solved by the introduction of a scaling term within the cost function; the convergence of the conjugate gradient algorithm is improved with the use of algorithm resetting; and finally, *a priori* knowledge of the region of support of the object is replaced by a simple classification procedure. We hope that this paper will inspire further research on the NAS-RIF algorithm.

Acknowledgment

References

[1] D. Kundur and D. Hatzinakos, "Blind image deconvolution," *IEEE Signal Processing Mag.*, vol. 13, pp. 43–64, 1996.
[2] D. Kundur and D. Hatzinakos, "Blind image deconvolution revisited," *IEEE Signal Processing Mag.*, vol. 13, pp. 61–63, 1996.
[3] M. R. Banham and A. K. Katsaggelos, "Digital image restoration," *IEEE Signal Processing Mag.*, vol. 14, pp. 24–41, 1997.
[4] G. R. Ayers and J. C. Dainty, "Iterative blind deconvolution method and its applications," *Opt. Lett.*, vol. 13, pp. 547–549, 1988.
[5] B. C. McCallum, "Blind deconvolution by simulated annealing," *Opt. Commun.*, vol. 75, pp. 101–105, 1990.
[6] D. Kundur, "Blind deconvolution of still images using recursive inverse filtering," M.A.Sc. thesis, Dept. Elect. Comput. Eng., Univ. Toronto, Toronto, Ont., Canada, 1995.
[7] C. A. Ong, "Blind image restoration using the NAS-RIF algorithm," M.Eng. thesis, Dept. Electr. Electron. Eng., Imperial College, Univ. London, U.K., 1997.
[8] E. Polak, *Optimization Algorithms and Consistent Approximations*. Berlin, Germany: Springer-Verlag, 1997.
[9] R. C. Gonzalez and P. Wintz, *Digital Image Processing*, 2nd ed. Reading, M: Addison-Wesley, 1987.
[10] A. K. Jain, *Fundamentals of Digital Image Processing*. Englewood Cliffs, NJ: Prentice-Hall, 1989.